

THE TERRAIN OF EVOLUTION OF ISOTROPIC ADIABATIC SUPERNOVA REMNANTS

DONALD P. COX

Rice University; and the University of Wisconsin, Madison

Received 1985 May 30; accepted 1985 November 6

ABSTRACT

Models of the evolution of supernova remnants in isotropic media are reviewed and generalized. It is shown that properties of remnants (including cooling and volume-filling aspects) are almost history-independent functions of their instantaneous average density and postshock temperature.

These properties, presented as a contour diagram in the density-temperature plane, thus define the territory through which remnant properties evolve. In different models, remnants merely take different paths across the available terrain.

For the Milky Way, M101, and the LMC, the portions of this terrain which might actually be sampled by the remnant populations are discussed briefly.

Subject heading: nebulae: supernova remnants

I. INTRODUCTION

When considering the effects of supernova remnants (SNRs) on the interstellar medium (ISM) and vice versa, there are useful subdivisions for the possible dominant behaviors. These can be segregated by considering the ultimate disposition of the supernova power. (Cosmic-ray acceleration and pV work done on very diffuse interstellar clouds probably receive modest fractions, but roughly half the supernova (SN) energy almost surely remains in the lowest mass density thermal component within the individual remnants as they evolve [e.g., Cox 1979]. It is with that portion that we are concerned.)

Three potential fates for this energy have been widely proposed. First, it may be radiatively dissipated by individual remnants evolving in the disk ISM. If, however, individual remnants do not become efficient radiators before overlapping with one another, the hot gas fills the plane and expands into the galactic corona. Two fates then remain. If the corona is sufficiently dense, the energy can be radiated. If not, it drives a galactic wind and is dispersed, along with the material, into the surrounding space.

Since there are three fates, there would seem to be two dividing lines, one separating galactic conditions leading to individual radiative remnants from those leading to remnant merger before cooling. The other line should separate conditions leading to radiative coronae from those leading to galactic winds.

Things are a bit more complicated than that, however. There are at least four types of galactic coronae. In order of mass flow (from high to low), they can be ordered as: fountains (as in Shapiro and Field 1976), quasistatic coronae, cold Parker winds, and hot supersonic winds. Which of these is to be expected depends very sensitively on the ratio of mass to energy flux entering the corona. It is so sensitive that any real disk galaxy probably ought to have a corona of mixed type, owing to nonuniformities in the source function and depth of the gravitational potential (Chevalier and Oegerle 1979; Bregman 1980*a, b*). Of the four types, fountains and quasistatic coronae dissipate the supernova power radiatively.

Having identified these regimes qualitatively, the next step is to establish the dividing lines between them in quantitative terms. What disk conditions lead to what situations? Those

segregations are the subject of the first two papers in this series, where they are explored in very general terms. The segregation among halo types for a given gravitational potential depends only on the mass and energy fluxes into the corona, not on the details of remnant evolution within the disk. The exploration of those parameters is postponed to Paper II (Cox 1986; preview in Cox 1985). The present paper concerns itself with the division between systems having isolated versus merging remnants.

The identification of this division is an extremely difficult problem unless one knows very specifically how individual remnants evolve in and interact with the highly inhomogeneous real interstellar medium. There have been a number of attempts to study all or part of this evolution's aspects under various assumptions about the structure of the ISM and the relative importance of processes such as thermal evaporation (e.g., Cox and Smith 1974; Heathcote and Brand 1983; Cox 1979; McKee 1983). The most complete analysis of this kind is probably that of McKee and Ostriker (1977, hereafter MO) as elaborated by Cowie, McKee, and Ostriker (1981).

All models attempted thus far have problems and strengths, and very likely none is especially representative of actual remnant evolution, at least not for all phases of all remnants. The MO analysis, however, contains a number of extremely valuable insights, independent of the particular evolution mode that one is imagining to take place.

One of those insights is that in a sufficiently inhomogeneous medium, the supernova disturbance maintains a more or less spherical form as it evolves around the denser features of the ISM. One expects this to be true once the remnant is larger in scale than the inhomogeneities while still smaller than the disk scale height. Another is that the general characteristics of that disturbance, while it is strong, are governed by quite simple physical relations (e.g., the expansion rate is like the internal sound speed, the temperature is like the average energy per gram, the pressure is like the energy density).

So much of the MO paper, however, is devoted to the details of their particular remnant evolution scenario that the great importance of their more general beginning deserves the reemphasis and more precise discussion provided by the remainder of this paper.

Section II presents detailed evolutions from Sedov (1959) as normalized by Cox and Franco (1981, hereafter CF) for point explosions in media with power-law radial density gradients. The remnant luminosities, radiated energy fraction, and shell formation epoch are established quantitatively. In addition, a filling fraction function is defined and evaluated, in order to establish conditions leading to the overlapping of remnants. Finally, the MO notion that evaporative remnants should behave similarly but with slightly enhanced radiative efficiency is invoked to bring that evolution scheme under the same algebraic umbrella.

Section III presents the results graphically for three extremely different cases but does so with somewhat unusual independent parameters: One generally considers how the evolution of a specific remnant depends on the surrounding density distribution and would logically follow the evolution as time progresses. During the evolution, the mean density within the hot interior of the remnant may increase (evolution in preexisting cavity), stay constant (evolution in homogeneous medium), or decrease (evolution with ever decreasing rate of thermal evaporation of clouds).

Another approach is to study properties of remnants with given conditions, looking at the family of possibilities rather than following individual behaviors. An excellent set of independent variables for such study is the instantaneous mean internal density and the postshock temperature. The latter is surely monotonic with age for every conceivable evolution, nicely replacing time as the clock for the individuals. These variables are desirable for two reasons. One is that they are directly connected to contemporary observations. When one studies a remnant, what one infers are densities, temperatures, and thus pressures. Also observable is the remnant radius, which when combined with the pressure determines the explosion energy. As a consequence, by presenting evolutions as functions of the explosion energy, the postshock temperature T_s , and the instantaneous mean density of hot gas in the interior \bar{n} , the only remaining uncertainty would be which of the evolution types the remnant was following. Everything else is tied to the observations.

The second reason that these are desirable variables follows from studying the contour plots on the (\bar{n}, T_s) -plane of radius, age, luminosity, fraction of energy radiated, shell formation epoch, and overlap conditions for the different types of evolutions. *These plots show only small differences from one another, the biggest differences being in the age and radiated fraction loci.* What that means is that the important aspects of remnant condition can be regarded almost as *local functions* of \bar{n} and T_s independent of the evolution that brought a remnant to that condition.

There is effectively one terrain of conditions in the (\bar{n}, T_s) -plane, with boundaries to that terrain at the lower temperatures. At high \bar{n} , the boundary is provided by shell formation as the remnants go radiative. At lower \bar{n} , the boundary is provided by overlapping of the large-scale remnants with one another.

Within this territory, evaporative remnants, homogeneous remnants, and cavity reheating remnants follow very different tracks. Real remnants may follow yet other tracks, possibly not even monotonic is \bar{n} versus T_s . But the terrain and boundaries are essentially the same. The aspect of this terrain and its determination of the dividing line between systems with independently cooling remnants and those with merging remnants are discussed in § IV.

The effort as a whole has several modest but useful results. It is the first algebraically complete and numerically precise presentation of the more general class of Sedov evolutions (although one must turn to CF for the interior structure and evolution of the electron temperature). It further includes the late radiative properties and evaluates the shell formation epoch carefully. It introduces areal (rather than volume) filling factors for the overlap analysis, consistent with the remnant sizes involved. It evaluates the (\bar{n}, T_s) -terrain for SNR evolutions and provides confidence in the applicability of this in discussions of the characteristics of real remnants evolving with unknown density histories. Finally, there is a brief discussion of some observational information regarding the regions of the (\bar{n}, T_s) -phase sampled by remnants in the Milky Way, M101, and the LMC.

II. THE DETAILED EVOLUTIONS

The self-similar structures of adiabatic point explosions in isotropic media with power-law density gradients were discussed by Sedov (1959). Using energy and emissivity integrals performed by CF for cases of positive density gradient and a cooling time estimation scheme due to Kahn (1976), the gross numerical properties of such explosions are here reviewed. The results are presented with temperature and average internal density as the free parameters, emphasizing the similarity among the general properties, even with very different gradients. An approximate evolution of "evaporative remnants" is included as well, fitting very nicely into the same picture.

Defining the density gradient such that the ambient density is

$$\rho_A(R) \propto R^b,$$

where $b = -\omega$ in former notations, the energy integral results can be approximated as

$$R_s^5 = \left(1 + \frac{b}{5}\right)^2 \frac{2.025 E_0 t^2}{\bar{\rho}(1 + 0.239b)},$$

where E_0 is the explosion energy, t its age, $\bar{\rho}$ its average internal density, and R_s is the radius of the shocked region. Note that $\bar{\rho} = 3\rho_A/(3+b)$, and that $R_s \propto t^{2/(5+b)}$.

Defining $\chi = (n + n_e)/n$ and $m = \rho/n$, where n is the number density of nuclei, we have the usual strong shock (in $\gamma = 5/3$) relations: $\rho_2 = 4\rho_A$, $p_2 = 3\rho_A v_s^2/4 = 4\chi n_A k T_s$, and the velocity relation $v_s = [2/(5+b)]R_s/t$.

By approximating the cooling coefficient with the usual $L \approx 1.3 \times 10^{-19} T^{-1/2}$ fit to the Raymond, Cox, and Smith (1976, hereafter RCS) result over the temperature range $4 \times 10^5 < T < 5 \times 10^7$ K, we can estimate remnant luminosities and locate the shell formation epoch. (Cox and Anderson 1982, hereafter CA, showed that for $b = 0$, the equilibrium L was a reasonable approximation so long as T_s was less than a factor of 10 above that at the shell formation locus.) The luminosity of a remnant is

$$\mathcal{L} = \int_0^V L n_e n_H dV \approx \int_0^V L n^2 dV = \beta L(T_s) N n_A$$

or

$$\mathcal{L} \approx \beta'(b) L(T_s) V \bar{n}^2,$$

where V is the remnant's volume. From integrals performed in CF, assuming $L(T) \propto T^{-1/2}$ as in the above approximation, we

have

$$\beta' = [(3 + b)/3]\beta \approx 4(3 + b)^2/(19 + 8b).$$

This provides an approximation to the luminosity which is proportional to $T^{-1/2}V\bar{n}^2$, $R_s^{(9+5b)/2}$, or $t^{(9+5b)/(5+b)}$. The fraction of the total energy which has been radiated by time t is thus

$$f = \int_0^t \frac{\mathcal{L}(t)dt}{E_0} = \frac{5+b}{2(7+3b)} \frac{\mathcal{L}(t)t}{E_0}.$$

A number of complications to the above picture, including the equilibration time scale for electron and ion temperatures, the central plateau electron temperature if electrons are not shock-heated to the ion temperature, estimated effects of non-equilibrium ionization on the luminosity, and moderate structural changes brought about by thermal conduction are discussed in CA, CF, Cox and Edgar (1983), Edgar and Cox (1984), and references therein.

Collecting these results and expressing each parameter with \bar{n} and T_s as the independent variables,

$$R_s = \left[\frac{3(2.025)E_0}{100\chi k\bar{n}T_s(1+0.239b)} \right]^{1/3} \\ = 19.28 \text{ pc} \left[\frac{E_{51}}{\bar{n}T_6(1+0.239b)} \right]^{1/3},$$

$$v_s = \left(\frac{16\chi kT_s}{3m} \right)^{1/2} = 269 \text{ km s}^{-1} T_6^{1/2},$$

$$t = \frac{2}{5+b} \frac{R_s}{v_s} \\ = 2.8 \times 10^4 \text{ yr} \frac{5}{5+b} \left[\frac{E_{51}}{\bar{n}T_6(1+0.239b)} \right]^{1/3} \frac{1}{T_6^{1/2}},$$

$$\mathcal{L} = \beta' L(T_s) V \bar{n}^2 \\ = 1.15 \times 10^{38} \text{ ergs s}^{-1} \left[\frac{\beta' E_{51} \bar{n}}{T_6^{3/2}(1+0.239b)} \right],$$

$$f = \frac{5+b}{2(7+3b)} \frac{\mathcal{L}t}{E_0} = 3.62 \times 10^{-2} \\ \times \frac{7}{7+3b} \frac{\beta'(E_{51}\bar{n}^2)^{1/3}}{T_6^{7/3}(1+0.239b)^{4/3}}.$$

The absurd accuracy implied by these equations was retained only for making checks among the relationships. The numerical forms assume a helium to hydrogen number density ratio of 0.1. In addition, $E_{51} = E_0/10^{51}$ ergs and $T_6 = T_s/10^6$ K.

A very good approach for locating the onset of significant deviation from adiabaticity was found by Kahn (1976). He showed that when $L \propto T^{-1/2}$, the cooling time of a gas parcel is independent of its particular pressure and density history. For a gas parcel initially at density n_A , shocked to a density of $4n_A$ and temperature T_s , the time then required for cooling is

$$\Delta t_c = \frac{\chi k T_s}{4n_A L(T_s)}.$$

Adding this to the time at which the parcel was shocked specifies the age of the remnant when that parcel completes its cooling. By minimizing that sum, one learns the moment when

the first parcel to cool does so: that parcel first enters the shock at an epoch (parameters with subscript 1) for which

$$\frac{\chi k T_{s,1}}{4L(T_{s,1})n_{A,1}} = \frac{5+b}{9+5b} t_1.$$

It completes its cooling at time

$$t_c = \frac{2(7+3b)}{9+5b} t_1,$$

and most of the material in the outer part of the remnant cools very rapidly thereafter. Thus, t_c is the time marking the onset of shell formation, dramatically ending the adiabatic era. Remnant parameters at t_c satisfy

$$\frac{\chi k T_{s,c}}{4L(T_{s,c})n_{A,c}} \left[\frac{2(7+3b)}{9+5b} \right] \frac{2(7+3b)}{(5+b)} = \frac{5+b}{9+5b} t_c,$$

from which

$$T_{6,c} \approx 0.95 \left(\frac{9+3b}{9+5b} \right)^{3/7} \left(\frac{E_{51} \bar{n}_c^2}{1+0.239b} \right)^{1/7} \\ \times \left[\frac{9+5b}{2(7+3b)} \right]^{[6(7+3b)]/[7(5+b)]}.$$

Cox and Smith (1974) introduced the important notion of porosity, or volume filling factor of remnants in the galactic disk. MO showed that with remnant evolution primarily in a very low density component, the filling factor for the population can be quite large. For supernova rates like those thought to apply to the Galaxy, however, remnant radii exceed the probable scale height of the supernova site distribution before overlapping with neighbors. For this reason, when discussing the possibility of remnant overlap, it is necessary to use a surface area (rather than volume) filling fraction. Defining

$$Q_A(t) = \frac{\int_0^t \pi [R(t')]^2 dt'}{\pi R_g^2 \tau_{\text{SN}}} = \frac{5+b}{9+b} \frac{R^2(t)t}{R_g^2 \tau_{\text{SN}}}$$

for a population of remnants with ages less than t , the likelihood that an arbitrary point in the plane is not within the perpendicular column of any of the member remnants is $e^{-Q(t)}$. The fractional surface area coverage is $1 - e^{-Q}$. Note that $(\pi R_g^2 \tau_{\text{SN}})^{-1}$ is the supernova rate per unit area of the galactic plane. Numerically,

$$Q_A = 8.57 \times 10^{-4} \left(\frac{9}{9+b} \right) \frac{E_{51}}{1+0.239b} \frac{1}{\bar{n}T_6^{3/2}} \\ \times \left(\frac{15 \text{ kpc}}{R_g} \right)^2 \left(\frac{30 \text{ yr}}{\tau_{\text{SN}}} \right).$$

For given b , \bar{n} and T_6 , Q_A is proportional to the supernova power per unit area, $E_0/(\pi R_g^2 \tau_{\text{SN}})$.

These formulae can be used not only for power-law ambient densities, but also as a reasonable approximation to the properties of evaporation-dominated remnants. The mean internal density in such remnants is characterized by $b = -5/3$. The details of the expansion depend on the relative rates of evaporation and drag acceleration of the clouds, but properties cannot differ drastically from those found above. The only exception is that the general formula probably underestimates β' . In the discussion below, $\beta' = 2$ was assumed to be more reasonable. A very elaborate example of the evolution of

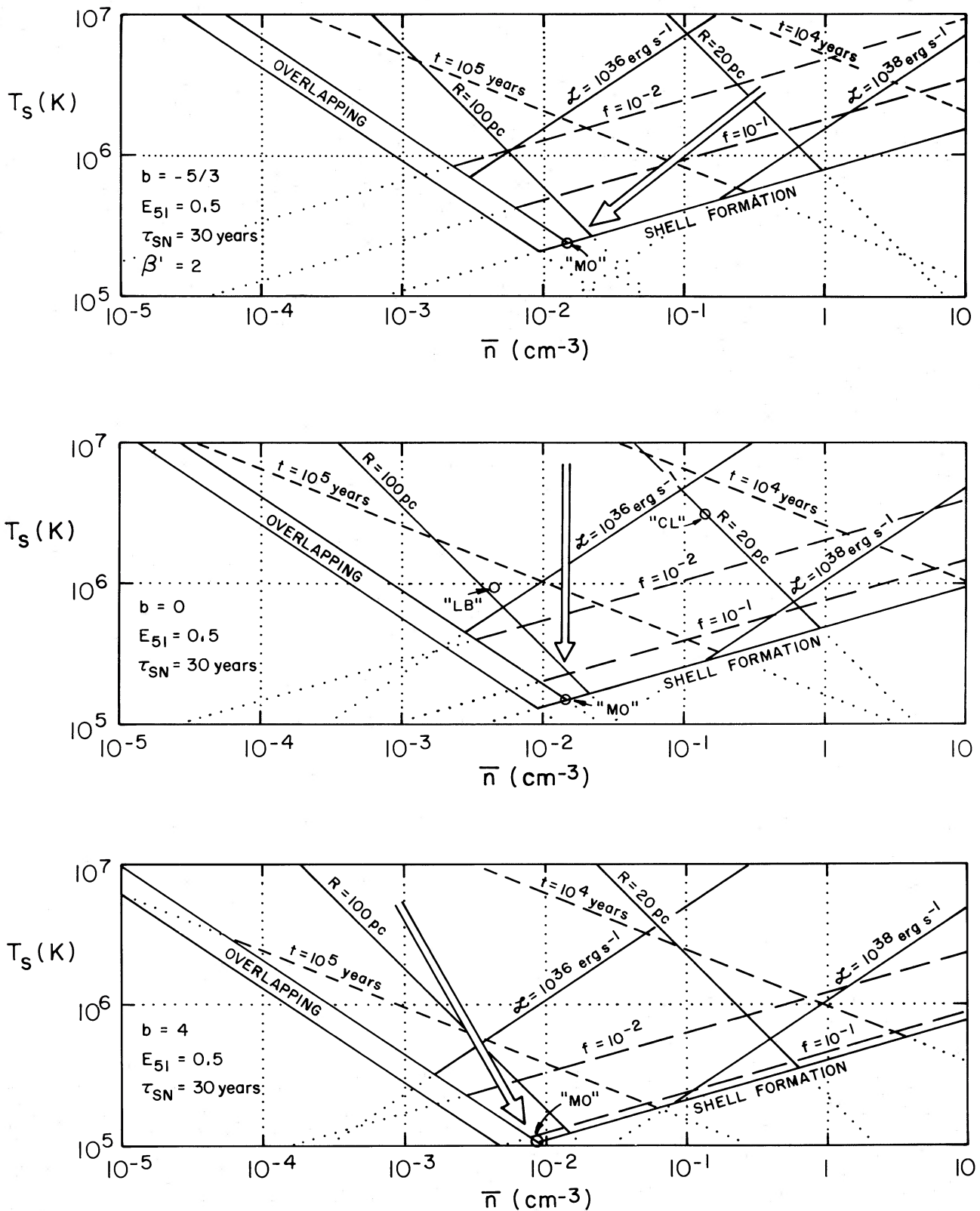


FIG. 1.—The terrain of evolution. Examples all assume $E_{51} = 0.5$, $\tau_{\text{SN}} = 30$ yr. Each is labeled with its assumed value of b , where mean density evolves as R^b . The vertical axis is postshock temperature; the horizontal is the average hot phase density interior to the remnant. Arrows indicate the slope of the evolutionary track for individual remnants. The band shown as “overlapping” is bounded on the top by $Q_A = \frac{1}{2}$ and on the bottom by $Q_A = 1$. The value of Q_A on such a line is proportional to the supernova rate. Thus the two lines more generally represent $Q_A \tau_{\text{SN}} = 15$ yr and 30 yr. The luminosities and integrated fraction of energy radiated f assume (an approximate fit to) the collisional equilibrium cooling coefficient. For $b = 0$ and T_s more than a factor of 10 above the shell formation locus, nonequilibrium ionization leads to higher luminosity than that shown.

such a remnant has been presented by Cowie, McKee, and Ostriker (1981).

III. THE TERRAIN OF EVOLUTION

Figure 1 presents the results of the above calculations for cases $b = 0$ (homogeneous), $b = 4$ (an example of evolution in cavities), and $b = -5/3$ (evaporation). For each, it shows loci of two radii, two ages, two luminosities, two radiated fractions, two area filling factors, and the shell formation epoch. Each diagram assumes the average supernova energy to be 5×10^{50} ergs, with a uniform rate per unit area of 1 per 30 yr in a disk of radius 15 kpc. Other diagrams are easily constructed from the formulae as provided. Individual remnants evolve in the region above the boundaries labeled as overlapping or shell formation. Only the location of the overlap boundary depends on population aspects such as the supernova rate or whether most remnants evolve with similar density histories. An arrow in each diagram indicates the slope of the track of individual remnants (for $b = 4$, $n \propto T^{-4/7}$, while for $b = -5/3$, $\bar{n} \propto T^{5/4}$).

For $b = 0$, representative remnant parameters that would provide the observed X-rays for the Local Bubble ("LB") and the Cyngus Loop ("CL") are indicated (e.g., Tucker 1971; Ku *et al.* 1984; CA; Edgar 1985). These two remnants are located at $R = 100$ pc and $R = 20$ pc respectively, more or less along the $\mathcal{L} = 10^{36}$ ergs s^{-1} locus. (The luminosities shown are total, not the often quoted \mathcal{L}_x . The ratio is strongly temperature-dependent and is shown for some bands in RCS.) If these two points were accurate representations of these remnants, then either different remnants evolve with very different density histories, or the mean density decreases rapidly with age. The latter tendency, of course, is characteristic of evaporative remnants. There are also indications of such a trend at higher density in the remnants of the Large Magellanic Cloud. The appearance of such a trend might also arise largely from selection effects. It could be due in part to a hierarchical distribution of interstellar matter so that noticeable remnants encounter lower prevalent density with increasing scale.

The two loci shown for overlapping correspond to Q_A of $\frac{1}{2}$ and 1. The intersection of the shell formation locus with $Q_A = 1/2$ is marked "MO." For $b = -5/3$ it corresponds most closely to the remnant end point espoused by MO. Its generalization for other values of b is labeled in recognition of the MO identification of this extremely important crossing. In all cases this marks the critical division of possibilities: for galactic systems whose remnants follow tracks ending to the right of this point, remnants evolve independently, form shells, and radiate their energies before noticing one another. The characteristic temperature of that radiation can be read from the graph; unless the system density is extremely high, the bulk of the radiation is in the EUV. On the other hand, for galactic systems with such low interaction densities that remnant tracks end to the left of the MO point, the ultimate disposition of the supernova power is a collective process among merged remnants. Such systems necessarily have an active halo or corona, charged with the dispersal of the supernova power. The forms of such coronae and the boundary conditions they would place on the disk are the subject of a companion paper (Cox 1985, 1986).

The information in Figure 1 is not particularly surprising, and for the most part is contained in the algebraic formulation of MO. For a given explosion energy, the postshock temperature is inversely proportional to the enclosed mass. Hence,

for a given T and \bar{n} , the radius is fixed. The expansion velocity is proportional to $T^{1/2}$, and the remnant age is a fraction of R/v . The quantities graphed are just combinations of these parameters that depend on T and \bar{n} in obvious ways. The action of the density evolution, represented by b , is to alter the constants of proportionality slightly. The extent to which the unknown details of the actual evolution of remnants can be expected to differ from Figure 1 can thus be judged from the degree of difference between the three versions presented. These represent drastically different histories of individual remnants.

Several small remarks are in order as one studies Figure 1. (1) The track inferred for the Local Bubble is noticeably to the left of the critical "MO" track, unless the evolution is taking place in a rather steep-walled cavity. (2) In all cases, overlap occurs only after remnant radii exceed 100 pc, establishing the need for an area (rather than volume)-dependent criterion. (3) Shell formation at $R = 100$ pc corresponds to $Q_A \approx \frac{1}{4}$ in every case, with \bar{n} close to 2×10^{-2} cm^{-3} . For different assumed supernova rates, the values of Q for the lines shown vary in direct proportion to the rate. Thus $Q_A = \frac{1}{2}$ for $\tau_{SN} = 60$ yr has the same line as $Q_A = 1$ for $\tau_{SN} = 30$ yr. (4) For $b = -5/3$, remnants evolve at nearly constant luminosity. (5) At the lower temperatures, the approximate cooling function used in making the diagram overidealizes a bit, being as much as a factor of 3 lower (at 2×10^5 K) than the collisional equilibrium cooling function. The propriety of the equilibrium function prior to shell formation is discussed by CA. (6) Apart from the tracks taken by individual remnants, the similarity among these diagrams is much more apparent than the differences. This encourages the sense that the natural analog might be well represented by a similar diagram.

Figure 2 is identical to Figure 1 except that the higher supernova energy $E_{51} = 1$ was assumed. For the same total power, the $Q_A = 1$ line of Figure 2 should be compared with the $Q_A = \frac{1}{2}$ line of Figure 1.

IV. DISCUSSION

The usefulness of Figure 1 is vaguely like that of a topographic map. Individual remnants may follow very complex paths in the diagram. Some may occur initially in regions of unusually high density, break out, or gradually evolve into lower density. Some may begin their evolutions in the cavities of previous remnants or wind bubbles, eventually growing to interact with the higher density surrounding material. At very large scale, remnants may break out of the higher density disk and evolve rapidly until they merge in the lower corona. What the near invariance of the diagram provides is confidence that although remnants in general have unknown trends in their evolutions, and specific remnants may evolve quite differently, one still knows the topography through which the gradual portions of the evolution take place and the locations of the boundaries to the accessible territory.

This kind of knowledge is particularly useful if the majority of remnants eventually reach a common track, for example evolution in a particular density at very large scale. It would then be reasonably clear that the population properties of the large-scale remnants were only very weakly dependent on the early evolution histories of the individual members.

The diagram is still useful without such a simplifying condition. It establishes the shell formation epoch for individual remnants, almost without regard to their individual paths, as well as providing a useful visualization of the two-dimensional

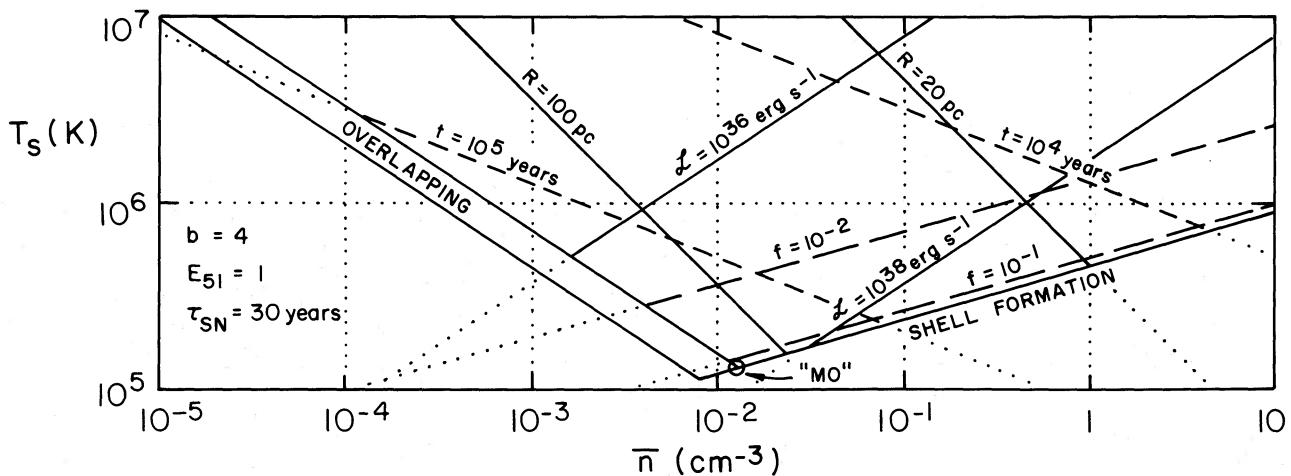
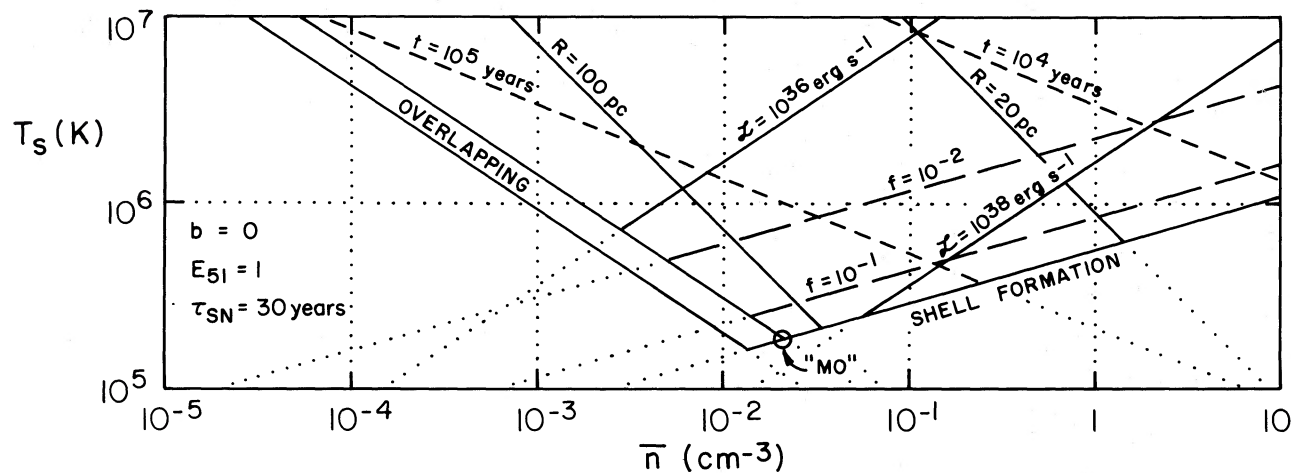
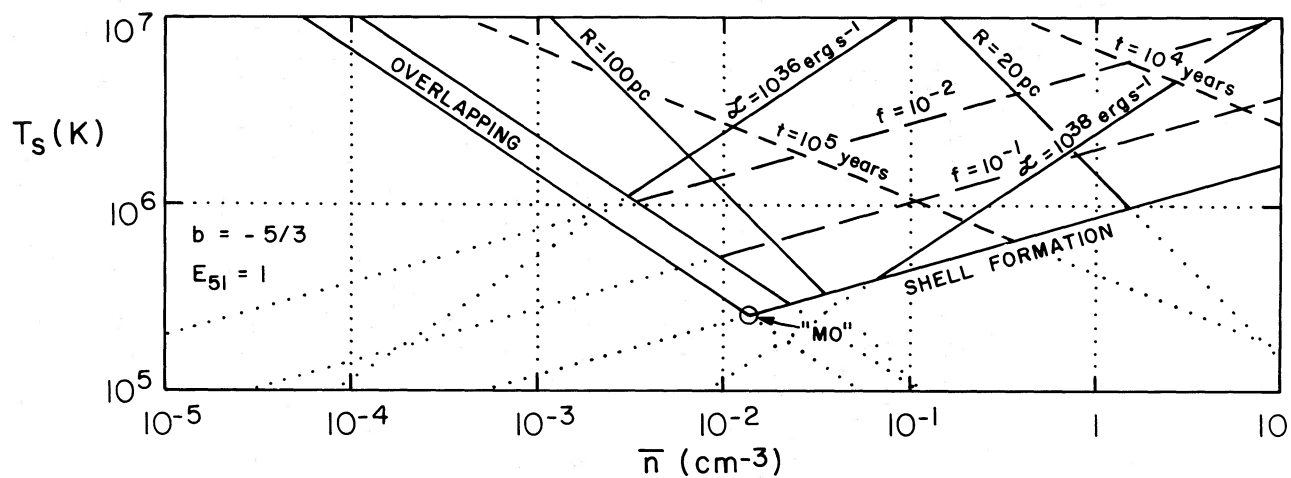


FIG. 2.—Same as Fig. 1 except $E_{51} = 1.0$.

parameter space to which adiabatic remnant properties are constrained.

The total mass with which a supernova shares its energy prior to either overlapping with neighbors or undergoing shell formation can easily be inferred from the lowest temperature reached. (The diagrams can be visually normalized to mass by noting that the intersection of $R = 20$ pc with $n = 1 \text{ cm}^{-3}$ encloses $1000 M_{\odot}$, while $R = 100$ pc at $\bar{n} = 10^{-3}$ encloses $125 M_{\odot}$.) It is apparent that the maximum mass interaction occurs for remnants evolving to the MO point, about $3000 M_{\odot}$, and that the total interaction mass depends only weakly on \bar{n} along the shell formation boundary. Shell formation at even a relatively high density of $\bar{n} = 1 \text{ cm}^{-3}$ still involves having heated $1000 M_{\odot}$, although much earlier in the remnant's history.

In constructing this diagram, it has been assumed that the average density of hot material within the remnants in a galaxy could take on any value. The consequence for the remnants of any particular density or evolution are then apparent.

In point of fact, the relevant density derives directly from circumstances and processes within the disk that determine the rate at which supernova remnants remove material from denser components of the interstellar medium. In the original MO model, these processes were sufficiently deterministic that the system as a whole conspired to drive remnants along the evolutionary track leading to the MO point. *Without denying the likelihood of some such determinism*, the approach taken in the present series of papers allows the exploration of a broader range of possibilities. For examples, we now turn briefly to results of three relevant studies of different galactic systems.

In the case of the Milky Way, Cowie and York (1978) have found an important observational limit on the mean density with which remnants interact during the *radiative* (or snowplow) phase. By studying the distribution function of components of strong UV absorption lines in stellar spectra, they show that, if remnants become radiative before overlap, the low-component frequency observed for the solar neighborhood is consistent only with

$$n > 0.1(2E_{51})^{0.85}(30 \text{ yr}/\tau_{\text{SN}})^{0.89} \text{ cm}^{-3},$$

where τ_{SN} is the mean time between SNs in a disk of radius 15 kpc and thickness 200 pc.

This limit applies equally to all diagrams (any b) for evolution below the shell formation boundary. By comparing it with Figures 1 and 2, the limit is seen to exclude a factor of 10 in density above that at the MO point. Densities lower than the MO value are not excluded because there are then no radiative remnants. Thus the results do not distinguish whether the intercloud ISM is predominantly hot and low in density, perhaps with MO-style evolution of its remnants, or merely warm and higher in density (e.g., Field, Goldsmith, and Habing 1969); at least they do not allow a noncommittal intermediate.

For M101 the observational situation is somewhat different. Cox and McCammon (1986) studied the upper limit to the X-ray surface brightness of this galaxy (McCammon and Sanders 1984) and concluded that both upper and lower limits could be set on the density with which remnants interact. For $b = -5/3$, the density limits are mutually exclusive unless the supernova power per unit area is somewhat lower than expected. For what might be regarded as a reasonable lower bound on the supernova power, the MO state is marginally possible at the upper limit to density. For $b = 0$, however, the allowed range of possibilities is not so constrictive.

Representing the supernova rate per unit area with $r =$

$(15 \text{ kpc}/R_g)^2 (30 \text{ yr}/\tau_{\text{SN}})$, the allowed density range is

$$0.01 \text{ cm}^{-3}(E_{51} r)^{1.2} < n < 0.023 \text{ cm}^{-3}(E_{51}^2 r)^{-1.5}.$$

The apparent narrowness and low values of this range with $E_{51} = r = 1$ are deceptive. For $E_{51} = 0.5$, $r = 1$, the range runs from 4×10^{-3} to 0.2 cm^{-3} eliminating no interesting possibility. In short, for $b = -5/3$, the MO state is marginally allowed if $E_{51}^{29/26} r < 0.09$, while for $b = 0$, the density range extends up to 0.1 cm^{-3} only for $E_{51}^2 r < 0.38$.

If one assumes $b = 0$ and, however ill advised, that the Cowie and York (1978) and Cox and McCammon (1985) limits could both be applied to either galaxy, then the combined effect is either that the density is too low for individual radiative remnants (but not in the range that would make the corona X-ray bright) or that it satisfies

$$0.1 \text{ cm}^{-3}(2E_{51})^{0.85}r^{0.89} < n < 0.2 \text{ cm}^{-3}[(2E_{51})^2r]^{-1.5}.$$

Quirkily enough, the the two points in Figure 1 representing the X-ray properties of the Local Bubble and the Cygnus Loop fall one each in the two different allowed density ranges.

The final example is the supernova remnant population of the Large Magellanic Cloud. The observations (many collected in Mathewson *et al.* 1983) have caused considerable surprise and loss of confidence in simple models such as those in this paper. In particular, from a nearly linear number-versus-diameter relation, the remnants would appear to have a prolonged period of free expansion (e.g., Mills 1983). In addition, from a straightforward thermal analysis of the X-ray emission, the LMC remnants would seem to evolve such that their thermal energy increases with diameter while the mean internal density decreases (Long 1983). Of course, such conclusions are based at least loosely on an inherent assumption that the observed remnants are a suitably complete representation of an evolution sequence.

The statistics are certainly misleading: by annotating a map of remnant locations with properties of the remnants, one quickly finds patterns in the type of remnants found in different locations. For example, of the large remnants with low X-ray luminosity, all but one are found on the periphery, most either south of the midline of the stellar bar or beyond its ends, two on the eastern periphery and one on the far north. Next, a 2° wide band north of (and parallel to) the midline of the bar contains all three center-filled (somewhat Crab-like) remnants, all four Balmer-dominated remnants, the remarkable N132D, and the remaining large remnants of intermediate X-ray brightness. Two degrees further north yet are the three remaining very bright remnants N63A, N49, and N49B. Finally, the single remnant showing little or no X-ray emission but only modest size, N11L, is isolated in a dense region in the northwest.

Between the 2° swath just north of the bar and the bright remnant cluster in the far north is a pronounced zone of avoidance.

The considerable spatial variation of the type of remnant observed almost certainly depends on differences in relative rates of Types I and II supernovae between dense star-forming regions and peripheral regions, on the typical density within which the evolutions take place, and on the local background level of Lyman continuum. The sample not only does not represent a single evolutionary sequence, it can hardly be complete to the same limiting diameter over the entire face of the galaxy. (See Hughes, Helfand, and Kahn 1984, for a complementary approach supporting similar conclusions.)

Concerning ourselves only with information about the ISM densities sampled by the remnants, there are some fairly clear results. First, of all the remnants whose emission appears thermal, none fall in a region of the X-ray luminosity versus diameter plot that is not accessible to remnants of energy 5×10^{50} ergs, in densities which are reasonable for their locations. Thus, as a first pass we will compare only to models with that energy, $b = 0$ for simplicity, and abundances reduced by a factor of 4 from solar. Starting with the assumption that all remnants are in the adiabatic phase, the inferred ISM densities run between 0.03 cm^{-3} and $\sim 10 \text{ cm}^{-3}$. (These densities are similar to those shown in Long 1983, corrected slightly for abundance and nonequilibrium effects on the luminosity.) For the four Balmer-dominated remnants, for which the adiabatic phase assumption is probably valid, the inferred ambient densities are 0.2, 1.5, 3, and 10 cm^{-3} . The lowest density of these is found well outside the southeastern end of the bar, the intermediate densities are close together at the northwestern end of the 2° swath, and the densest is along the northern middle edge of the bar where the density certainly appears to be higher.

The remaining bright thermal remnants may have their emission enhanced by a reverse shock in the enriched ejecta, or their emission pattern and rate distorted by evolution in either a very inhomogeneous medium or a wind-blown cavity. Despite those potential complications, however, their densities do not appear surprisingly out of line. The three brightest (N49, N63A, and N132D) all show apparent ISM densities of 3 cm^{-3} . At that density (and the reduced abundances), shell formation should take place at a diameter of ~ 30 pc. N132D approaches that diameter and, although centrally complicated, probably shows the signs of a radiative shock wave on much of its perimeter. The other remnant in this class, N49B, appears larger and less dense (0.5 cm^{-3}). It is comfortably smaller than the shell formation diameter at this lower density but larger than that at the higher density of the others. Since the edge emission appears lumpy, with only marginal indication of shell formation on some directions, the lower density is probably more typical. A Balmer-dominated edge is not seen, but perhaps it is hidden in the confused emission from the region, or the surrounding gas is already ionized.

It is of some interest to consider the possibility that the lowest luminosity remnants are truly indicative of regions with densities considerably below the 0.2 cm^{-3} shown by the least dense Balmer-dominated remnant. First, very low densities are easily kept ionized, so that absence of Balmer-dominated shocks is not surprising. Second, most of these remnants are sufficiently large that the pressures within them are incapable of driving X-ray emitting shocks into any high-density clouds that should happen to be included within them. Third, however, several of these remnants show signs of extensive development of radiative shocks along their boundaries (e.g., DEM 249, DEM 238, N86; perhaps N206 and N120, both of which appear to be in denser environments). Fourth, in at least some cases the morphology of the emission indicates that there were significant perturbations in the presupernova ambient density distribution that contributed to the growth of these remnants to the large sizes observed (e.g., DEM 299, N86, DEM 204, N135). Next, the luminosities of this class of remnant are consistent with the emission expected from the diffuse interior of a remnant shortly after completion of shell

formation. Such emission can be surprisingly hard, owing to a contribution from recombination of highly ionized metals. Finally, the sizes are consistent with shell formation in densities ranging from 0.5 cm^{-3} (for DEM 204) to 4 cm^{-3} (for N120).

Thus, there is no clear evidence that any of the observed remnants is evolving in a region whose ambient density is significantly less than 0.2 cm^{-3} , except perhaps within limited confines of preexisting cavities about the explosion sites. Most of the larger remnants are consistent with evolution in an ambient density of roughly 1 cm^{-3} . Most of the smaller bright remnants are consistent with ambient densities only moderately higher ($\sim 3 \text{ cm}^{-3}$), with enough scatter that there is some overlap between the two populations. The spatial distribution is consistent with the lower density being prevalent only on more peripheral regions, while even higher densities may be present in the zone of avoidance, leading to very transient visibility or total invisibility. An example is the remnant N11L, which is apparently in a dense complex, has only moderate diameter (~ 15 pc), but shows very little X-ray emission (from its being well past shell formation, or heavily absorbed, or still within a preexisting cavity).

From this discussion one tentatively concludes that the LMC remnants evolve in sufficiently high densities that their fate is shell formation rather than overlap and the generation of a hot corona.

The remnant models studied here are characterized in the title as isotropic. The reason for the labeling is that there are ways that remnants could evolve that would not be well represented in Figure 1. What is required is a decoupling of the rates of growth and radiation. In a medium with irregularities on scales of the size of a remnant, growth of the remnant (after thermalization) takes place at a rate characterized by the lowest density broadly available. At the same time, the radiation rate depends on the broad availability of higher densities. Since one uses the radiative properties to infer densities, temperatures, and pressures, the growth rate will likely be underestimated and the age overestimated. Such remnants share some characteristics with those in homogeneously inhomogeneous media as in MO or Cowie, McKee, and Ostriker (1981), but for the most part their evolution remains unexplored territory. (See, however, McKee 1983 for a thorough beginning.) Unfortunately, recent attempts to understand specific remnants such as the Cygnus Loop in detail (e.g., Hester, Parker, and Dufour 1983; Hester and Cox 1986) are tending toward interpretation in decidedly anisotropic terms. One knows, of course, from the obvious irregularity of the interstellar medium in general that this is a problem that must one day be wrestled.

The second paper in this series will be a discussion of the boundary conditions provided to disks by active coronae in systems evolving to the left of the MO point. The third will consider ISM conditions brought about by remnant evolution in systems to the right of the MO point.

This material is based on work supported by the National Science Foundation under grant No. AST 84-15142. It was also supported in part by the National Aeronautics and Space Administration under grant NAG5-629. Reggie Dufour was very helpful in getting a perspective on the LMC remnants.

REFERENCES

- Bregman, J. N. 1980a, *Ap. J.*, **236**, 577.
 ———. 1980b, *Ap. J.*, **237**, 280.
 Chevalier, R. A., and Oegerle, W. R. 1979, *Ap. J.*, **227**, 398.
 Cowie, L. L., McKee, C. F., and Ostriker, J. P. 1981, *Ap. J.*, **247**, 908.
 Cowie, L. L., and York, D. G. 1978, *Ap. J.*, **223**, 876.
 Cox, D. P. 1979, *Ap. J.*, **234**, 863.
 ———. 1985, in *Proc. NRAO Workshop on Gaseous Halos of Galaxies*, ed. F. Lockman and J. Bregmann (Greenbank, WV: NRAO), in press.
 ———. 1986, in preparation.
 Cox, D. P., and Anderson, P. R. 1982, *Ap. J.*, **253**, 268 (CA).
 Cox, D. P., and Edgar, R. J. 1983, *Ap. J.*, **265**, 443.
 Cox, D. P., and Franco, J. 1981, *Ap. J.*, **251**, 687 (CF).
 Cox, D. P., and McCammon, D. 1985, *Ap. J.*, **304**, 657.
 Cox, D. P., and Smith, B. W. 1974, *Ap. J. (Letters)*, **189**, L105.
 Edgar, R. J. 1985, *Ap. J.*, submitted.
 Edgar, R. J., and Cox, D. P. 1984, *Ap. J.*, **283**, 883.
 Field, G. B., Goldsmith, D. B., and Habing, H. J. 1969, *Ap. J. (Letters)*, **155**, L149.
 Heathcote, S. R., and Brand, P. W. J. L. 1983, *M.N.R.A.S.*, **203**, 67.
 Hester, J. J., and Cox, D. P. 1986, *Ap. J.*, **300**, 695.
 Hester, J. J., Parker, R. A. R., and Dufour, R. J. 1983, *Ap. J.*, **273**, 219.
 Hughes, J. P., Helfand, D. J., and Kahn, S. M. 1984, *Ap. J. (Letters)*, **281**, L25.
 Kahn, F. D. 1976, *Astr. Ap.*, **50**, 145.
 Ku, W. H.-M., Kahn, S. M., Pisarski, R., and Long, K. S. 1984, *Ap. J.*, **278**, 615.
 Long, K. S. 1983, in *Supernova Remnants and Their X-Ray Emission*, ed. J. Danziger and P. Gorenstein (Dordrecht: Reidel), p. 525.
 Mathewson, D. S., Ford, V. L., Dopita, M. A., Tuohy, I. R., Long, K. S., and Helfand, D. J. 1983, *Ap. J. Suppl.*, **51**, 345.
 McCammon, D., and Sanders, W. T. 1984, *Ap. J.*, **287**, 167.
 McKee, C. F. 1983, in *Supernova Remnants and Their X-Ray Emission*, ed. J. Danziger and P. Gorenstein (Dordrecht: Reidel), p. 87.
 McKee, C. F., and Ostriker, J. P. 1977, *Ap. J.*, **218**, 148 (MO).
 Mills, B. Y. 1983, in *Supernova Remnants and Their X-Ray Emission*, ed. J. Danziger and P. Gorenstein (Dordrecht: Reidel), p. 551.
 Raymond, J. C., Cox, D. P., and Smith, B. W. 1976, *Ap. J.*, **204**, 290 (RCS).
 Sedov, L. I. 1959, *Similarity and Dimensional Methods in Mechanics* (New York Academic).
 Shapiro, P. R., and Field, G. B. 1976, *Ap. J.*, **205**, 762.
 Tucker, W. H. 1971, *Science*, **172**, 372.

DONALD P. COX: Department of Physics, University of Wisconsin-Madison, 1150 University Ave., Madison, WI 53706